Effect of Temperature Treatment on Electrical Property, Crystal Structures and Lattice Strains of Precipitated CaCO₃ Nanoparticles

Panya Khaenamkaew[a]* , Dhonluck Manop[a], Chaileok Tanghengjaroen[a] ,

Worasit Palkawong Na Ayuthaya[b]

[a]*Kasetsart University, Faculty of Science at Si Racha, Department of Basic Science and Physical Education, Si Racha Campus, Chonburi, 20230, Thailand*
[b]*Kasetsart University, Faculty of Science at Si Racha, Department of Resources and Environment, Si Racha Campus, Chonburi, 20230, Thailand*

In this study, the effect of temperature treatment during the preparation process of calcium carbonate (CaCO₃) nanoparticles was systematically examined for a drug delivery carrier. The CaCO₃ powder was prepared by the precipitation method at different annealing temperatures. The morphologies, elemental compositions and crystal structures of the synthesized CaCO₃ powder were analyzed by Scanning Electron Microscope/Energy-Dispersive Spectroscopy and X-ray Diffractometry (XRD), respectively. The result shows that the particle size increased with an increase in annealing temperature. Based on the crystal structure analyzed from XRD, the sample was perfectly matched with the calcite/ vaterite polymorphs phases. The crystallite size and lattice strains of the CaCO₃ powder were calculated from the full width at half maximum parameter. The results show that the increase in annealing temperature leads to an increase in crystallite size and a decrease in lattice strain. The CaCO₃ powder has a dielectric constant of 6.0–6.8 that reduced with the increase in applied frequency. The crystal structure, crystallite size, lattice strain, and dielectric properties of CaCO₃ powder are dependent of the annealing temperature. Such properties confirm that CaCO₃ powder is suitable for drug delivery carrier application.

Keywords: *CaCO₃ nanoparticle, crystal structure, lattice strain, dielectric constant, drug delivery carrier*

1. Introduction

Calcium carbonate (CaCO₃) is a major biomineral found abundantly in both organic and inorganic compounds[1]. CaCO₃ has wide applications in the fields of electronics, construction, medicine, plastic, cosmetics, and fillers[2,3]. Some forms of CaCO₃ nanoparticles serve as host materials for drug delivery carriers, sensors, chemical reactors[4,5], and nanofillers of CaCO₃/polymer composites [2,6]. Nanoparticle CaCO₃ fillers have an extremely large surface to volume ratio and may have considerably stronger reactions with the polymer matrix than their microparticle counterparts.

CaCO₃ exists in three polymorphic forms: calcite, vaterite, and aragonite. Calcite crystallizes in the hexagonal system, is stable at room temperature, and is the least soluble phase of the polymorphs. In comparison, vaterite crystallizes in the hexagonal crystal system and is the least stable polymorph, while aragonite polymorph crystallizes in the orthorhombic crystal system and is stable at high temperatures and pressures. These three phases have different lattice parameters that influence the properties and fabrication of the organic-inorganic compound[4]. The properties of CaCO₃ depend on certain variables such as pH, reaction temperature[4], concentration of solutions, concentration of additives, and type of additives[5]. However, to the best of our knowledge, the crystal structure and lattice strain of CaCO₃ powders

need further elucidation. The foremost challenge in using nanoparticle CaCO₃ powders is its potential use as drug carriers and fillers in the industry.

In previous studies, we reported the effect of reaction temperature on the particle size of CaCO₃ powder[7]. We found that the particle size, crystal structure and dielectric constant of the CaCO₃ powders depend on the reaction temperature. The vaterite phase is realized when the reaction temperatureis increased to 60ºC. The crystal formation will change from a cubic-shape and round-shape into a needle-like feature. To use nanoparticle CaCO₃ powder in the high-temperature condition, it is essential to evaluate the changes in its physical and mechanical properties under varying temperatures.

The objective of this article was to examine the influence of treatment temperature on CaCO₃ properties. The synthesis parameters, i.e., annealing temperatures, dielectric property, lattice strain, and average crystallite size, were also investigated to obtain a crucial condition yielding different phases of CaCO₃ polymorphs for applications in drug delivery and fillers.

2. Experimental Procedures

2.1 Synthesis of CaCO₃ polymorphs

CaCO₃ powders with different annealing temperatures were prepared using the precipitation method[6,8]. 0.2 mol/L

*e-mail: pkheanumkhaw@hotmail.com

of anhydrous sodium carbonate (Na_2CO_3; formula weight = 105.99 g/mol), purchased from Merck, KGaA, was dissolved in 200 mL of deionized water. The solution was gently dropped into dissolved calcium nitrate tetrahydrate ($Ca(Na_3)_2.4H_2O$; formula weight = 236.15 g/mol); the concentration and volume of the dropped solution remained the same as the Na_2CO_3 solution. The mixed solution was refluxed at different reaction temperatures of 20°C, 40°C, 60°C, and 80°C. The precipitated material was observed simultaneously as a white colloid in solution after mixing at each reaction temperature. The final particles of $CaCO_3$ were filtered using a Buchner funnel, thoroughly washed with distilled water, and then allowed to dry at room temperature. The $CaCO_3$ powder was divided and pelleted into a round plate form with a single axis hydraulic press at a pressure of 20.5±0.5 MPa in order to study the effect of annealing temperature on its electrical property. The round plate $CaCO_3$ samples were placed in a tubular furnace at different annealing temperatures of 300°C, 350° C, 400° C and 450° C for 3 hours with the heating rate of 3°C /min. The thickness and weight of the samples were measured to determine the density of the samples. The process is shown in Figure 1.

2.2 Analyses

The wide angle X-ray diffraction of the $CaCO_3$ samples was determined using a Rigaku benchtop X-ray diffractometer (MiniFlex 300/600, UK) with a monochromatized CuKα radiation in the diffraction range of 2θ = 20° to 80° [5,9]. In order to determine the crystallite size and lattice strain in the $CaCO_3$ powder, the width, β_r, of the diffraction peak after subtracting the instrumental effect can be considered as the sum of the widths due to the small crystallite sizes and lattice strain[10,11]:

$$\beta_r = \beta_{crystallite} + \beta_{strain} \quad (1)$$

The crystallite size L was calculated using the "Scherrer–Gottingen equation" from half-maximum width $\beta_{crystallite}$ of Bragg reflections observed in the diffraction angle (2θ)

$$\beta_{crystallite} = \frac{K\lambda}{L\cos\theta} \quad (2)$$

where K is a constant commonly assigned a value of unity (K=0.89), and λ is a wavelength of the CuKα radiation (l.5406 A°). The lattice strain can be represented by the relationship

$$\beta_{strain} = \eta\tan\theta \quad (3)$$

where η is the strain in the material. From Equations 1-3, the total width of the diffraction peak is as follows:

$$\beta_r = \frac{K\lambda}{L\cos\theta} + \beta_{strain} \quad (4)$$

$$\beta_r\cos\theta = \frac{K\lambda}{L} + \eta\sin\theta \quad (5)$$

Thus, the plot of $\beta_r\cos\theta$ against $\sin\theta$ will obtain a straight line with slope η, and the intercept $\left(\frac{K\lambda}{L}\right)$ will be the crystallite size (L).

The microstructure of the samples and their elemental compositions were examined by a field emission scanning electron microscopy (JEOL JSM model 7401, Japan). Gold and carbon were coated on the disc samples with a Pirani501 device for Scanning Electron Microscopy (SEM) and Energy-Dispersive Spectroscopy (EDS) analysis, respectively. EDS is used for elemental analysis or chemical characterization of a sample. It is based on the fundamental principle that each element has a unique atomic structure
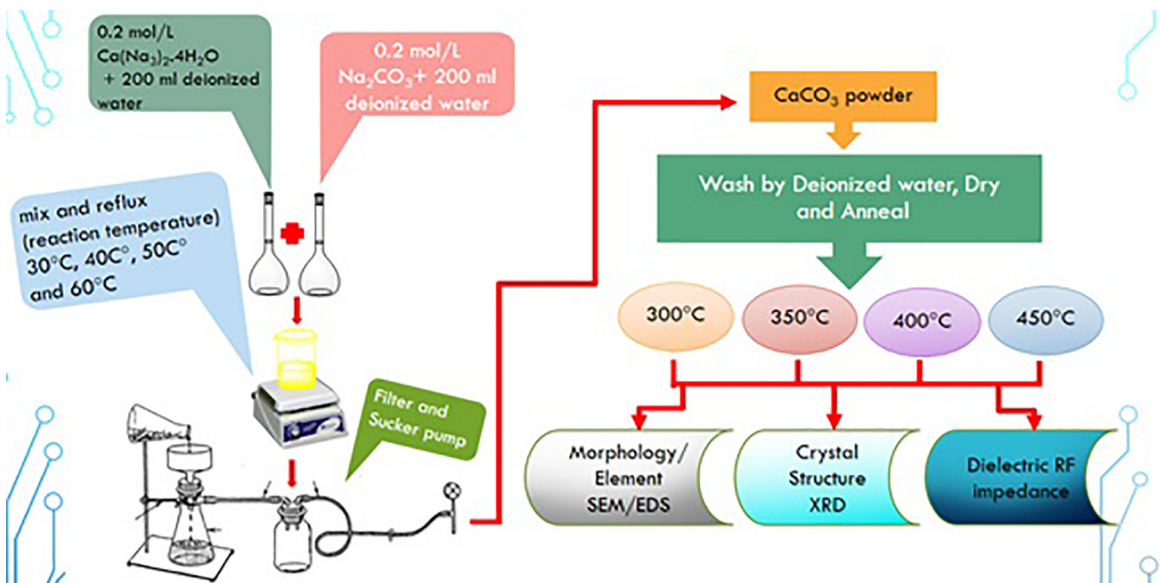

Figure 1. The diagram of $CaCO_3$ prepared by the precipitation method.

Effect of Temperature Treatment on Electrical Property, Crystal Structures and Lattice Strains of
Precipitated CaCO$_3$ Nanoparticles

3

that allows a unique set of peaks to be obtained on its electromagnetic emission spectrum, which is stimulated by a high-energy beam. The analytical conditions were adjusted to an acceleration voltage of 15 kV and 100 s of effective counting time.

The dielectric properties of the material provide valuable information about the storage and dissipation of electric fields in the materials and also provide the feasibility of using the material in potential applications. The dielectric constant is equivalent to relative permittivity (ε_r) or absolute permittivity (ε) relative to permittivity of free space (ε_0). The dielectric constant is generally a complex number that describes the interaction of a material with an electric field[12]:

$$\varepsilon = \acute{\varepsilon} - j\acute{\acute{\varepsilon}} = \acute{\varepsilon}(1 - j\tan\delta) = |\acute{\varepsilon}| e^{-j\delta} \qquad (6)$$

$$\acute{\varepsilon} = \varepsilon_0 \varepsilon_r \qquad (7)$$

$$\acute{\acute{\varepsilon}} = \acute{\varepsilon} \tan\delta \qquad (8)$$

The real part of permittivity (ε') is a measure of how much energy from an external electric field is stored in a material. In comparison, the imaginary part of permittivity (ε'') is called the loss factor and is a measure of how dissipative or lossy a material is to an external electric field. The loss factor includes the effects of both dielectric loss and conductivity.

The dielectric measurements of the desired CaCO$_3$ samples were taken by using the parallel plate method[13]. The parallel plate method involves sandwiching a thin sheet of material between two electrodes to form a capacitor. The equivalent circuit of the measurement is shown in Figure 2. The measured capacitance is then used to calculate permittivity. In an actual test setup, two electrodes are configured with a test fixture sandwiching dielectric material (RF Impedance analyzer Hewlett Packard: 4191A Dielectric Test Fixture, USA). The impedance measuring instrument would measure vector components of capacitance (C) and dissipation (D), and a software program would calculate permittivity and loss tangent as follows.
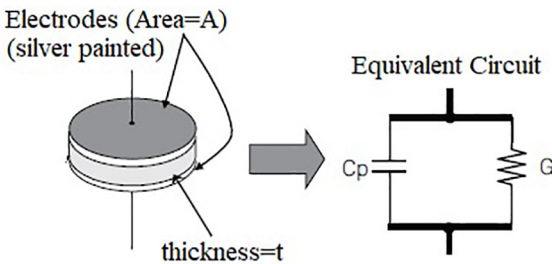

Figure 2. The equivalent circuit of dielectric measurement of round disc CaCO$_3$.

$$\acute{\varepsilon} = \frac{tC_P}{A\varepsilon_0} \qquad (9)$$

$$\acute{\acute{\varepsilon}} = \frac{t}{\omega R_p A\varepsilon_0} \qquad (10)$$

where t is the thickness and A is the area of the CaCO$_3$ samples.

3. Results and Discussion

3.1 Crystal Structure analysis by XRD

The X-ray Diffractometry (XRD) patterns of CaCO$_3$ samples with different annealing temperatures are shown in Figure 3. The XRD peaks observed in the control and treated samples exactly matched the reported values in the Joint Committee on Powder Diffraction Standards (JCPDS) card number no.00-024-0030 for CaCO$_3$ powder[3,5]. The most intense peak was observed at Bragg angles of 29.243°, 29.324°, 29.488°, and 29.324° in the samples treated at 300°, 350°, 400°, and 450°C, respectively. These peaks correspond to the crystalline plane (104) in treated samples; this is in agreement with the findings reported in the literature[14].
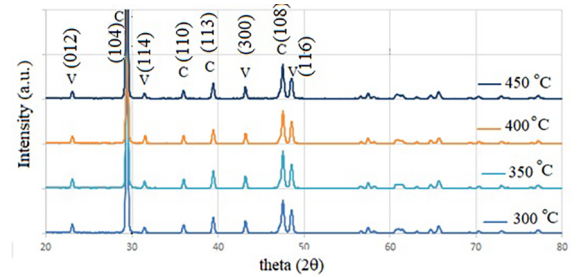

Figure 3. XRD patterns of CaCO$_3$ with different annealing temperatures.

Figure 3 confirms the calcite phase to be the most stable phase. However, no XRD peak for aragonite was detected in the desired CaCO$_3$ powders. From the XRD patterns relative to the annealing temperature, the desired CaCO$_3$ powders were found to be polymorphic mixtures of calcite and vaterite, and their characteristic peaks are stable with the annealing temperature. The polymorphic ratio (=phase fraction) of calcite to vaterite in the desired CaCO$_3$ powders was calculated based on the relationship between the peak intensities (I) at the characteristic faces and the abundance of the two polymorphs, as reported by Kim[15] and then expressed as a percentage fraction of calcite, X_C, as described in equation 11.

$$X_c \frac{I_{104(C)} + I_{110(C)} + I_{113(C)} + I_{108(C)}}{I_{104(C)} + I_{110(C)} + I_{113(C)} + I_{108(C)} + I_{012(V)} + I_{114(V)} + I_{300(V)} + I_{116(V)}} \qquad (11)$$

Table 1 shows the calculated phase ratio for different annealing temperatures of the desired CaCO$_3$ powders. From

equation 11, the phase fractions of calcite were found to be 83.22%, 89.60%, 82.20%, and 71.71% at the annealing temperatures of 300°C, 350°C, 400°C and 450°C, respectively.

The average nanocrystalline sizes were calculated using Equation 5 and the plots of $\beta_r \cos\theta$ against $\sin\theta$ (Figures 4a-4d). A linear relationship was observed between $\beta_r \cos\theta$ against of CaCO$_3$ powder. Table 2 shows the lattice parameters and the crystallite size of the CaCO$_3$ powder calculated from Equation 5. The average nanocrystalline sizes were found to be 10.54718, 9.14089, 8.56959 and 8.06549 nm and the lattice strains were 0.0039, 0.0024, 0.0019 and 0.0026 in the samples treated at 300° C, 350° C, 400° C and 450° C, respectively. In addition, a similar trend was observed in the crystallite size and lattice strain. Studies have reported that an increase in the temperature of CaCO$_3$ decreases crystallite size and lattice strain[10,16]. This reduction in lattice strain might reorient the neighboring planes in the same crystalline plane, resulting in a higher crystallite size in the treated sample compared to that mentioned in the literature[4]. However, the crystallite size and lattice strain are important indicators of the drug release process. In general, the smaller the crystallite size, the more the particles tend to be released. Similarly, the presence of more lattice strain in a plane (larger lattice mismatch) results in more instability. The above results indicate that the crystal structure, crystallite size, and lattice strain of CaCO$_3$ powders are dependent of the annealing temperature and are suitable for a host in the drug release process.

3.2 Microscopic Characterization of CaCO$_3$ by SEM

As mentioned in the previous paragraph, the SEM images (as shown in Figure 5) indicated the presence of both the cubic-shaped calcite and the round-shaped vaterite phases at an annealing temperature of 350°C. With the increase in annealing temperature, the crystal phase transformed into the circle-shaped vaterite phase, as shown in Figure 5b. These results are also consistent with the XRD investigation

that showed the calcite peak marked as "c" in Figure 3 to be gradually suppressed when the annealing temperature was increased from 350°C to 450°C. In comparison, the XRD results at annealing temperatures of 350°C and 400°C produced more calcite/vaterite than the aragonite/calcite phase; this is dissimilar to the findings obtained from SEM. This suggests that the morphologies of all three phases occur under normal temperature. However, due to the various thermal excitations during the process, one of the three possible forms can dominate, indicating the possibility of single-phase crystallinity. In addition, this result also agreed with the findings of Chen and Xiang[14]. In contrast, the SEM micrographs of CaCO$_3$ surfaces (Figures 5a-5b) revealed that the particle sizes of each powder were uniform and depended on the annealing temperatures, i.e., 300°C, 350°C, and 450°C. It was also revealed that the particle size of the CaCO$_3$ powder also depended on nucleation energy or growth energy. A lower reaction temperature needs more energy growth than a higher annealing temperature. This trend is similar to those reported in the literature[5].

Till now, a variety of nanoparticles, nanocrystallite sizes, nanocapsules and nanopolymer templates have been extensively studied as potential drug delivery systems. Size deviation, shape and morphology are related to stability, physicochemical performance such as dissolution and solubility, as well as cell uptake and final fate *in vivo* of nanosized materials, as already described in the literature[17,18]. In addition to the different morphologies and crystallite sizes, these carriers may have specific functionalizations on their surfaces to improve drug loading and controlled release and specific ligands for cell receptors, in order to achieve a precise targeting. In this study, the morphologies of the precipitated CaCO$_3$ powder are homogeneous at an annealing temperature of 300°C–400°C (Figures 5a-5c). This indicates that CaCO$_3$ powders are expected to be used for drug delivery. However, Figure 5d shows a nonhomogeneous morphology of the CaCO$_3$ powder at the annealing temperature of 450°C. This

Table 1. Calculated phase ratio vs. annealing temperature of desired CaCO$_3$ powders

Phases and planes	Intensity (a.u.) at different annealing temperatures				
	Commercial	300°C	350°C	400°C	450°C
v (012)	2555	1526	1461	1833	1114
c (104)	46887	52455	86860	45236	10045
v (114)	901	1446	1560	1262	607
c (110)	4437	2413	1947	2159	1429
c (113)	6117	4071	3256	3695	2341
v (300)	2839	3409	2892	3156	2009
c (108)	1980	1674	1491	1586	3248
v (116)	6687	5837	4945	5149	3001
Total intensity (a.u.)	72403	72831	104412	64076	23794
ΣI_c	59421	60613	93554	52676	17063
X_c	0.820698	0.83224	0.89601	0.82209	0.71711

Effect of Temperature Treatment on Electrical Property, Crystal Structures and Lattice Strains of
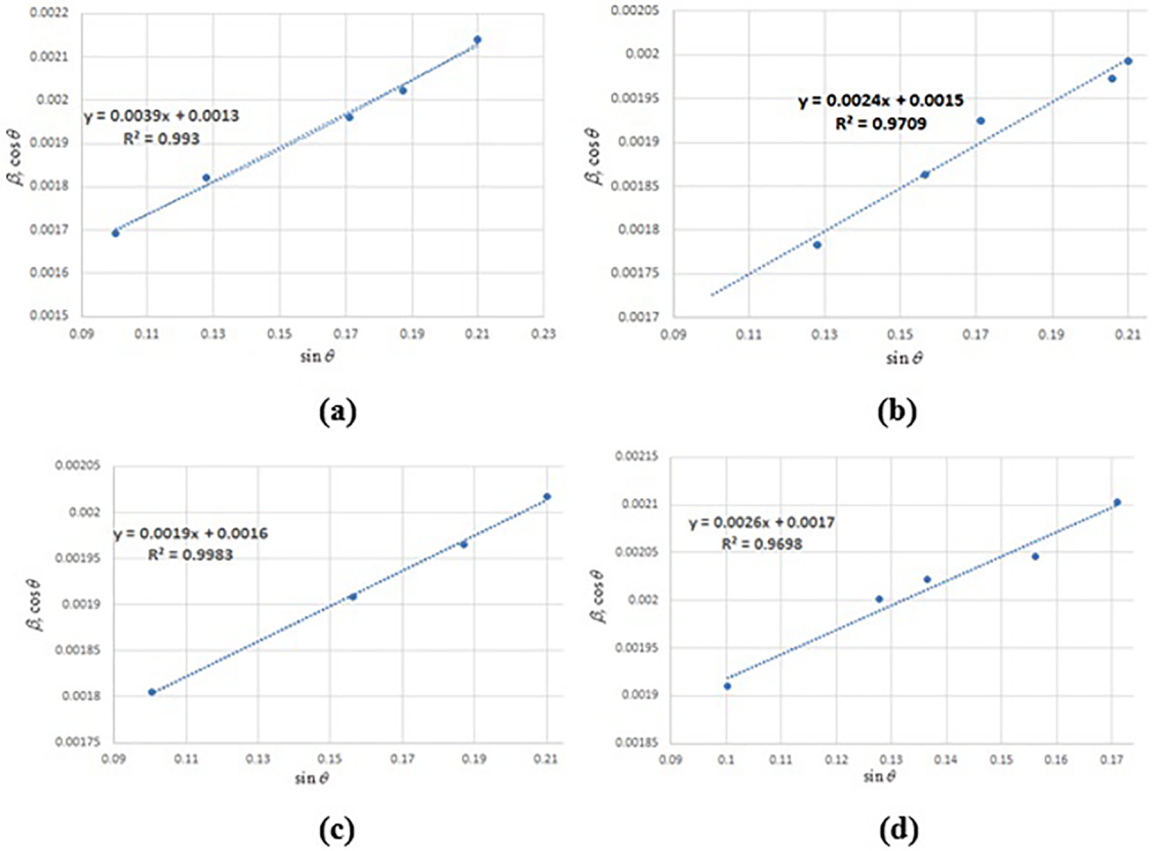Precipitated CaCO₃ Nanoparticles

5

Figure 4. Plot of $\beta_r \cos \theta$ against $\sin \theta$ of $CaCO_3$ annealed at (a) 300°C, (b) 350°C, (c) 400°C and (d) 450°C.

Table 2. Crystallite size and lattice strain versus annealing temperature of $CaCO_3$ powder

Annealing temp. (°C)	Latt.Cons.				
	(a: A°)	Latt.Cons. (c: A°)	Strain (η)	Intercepts ($\frac{K\lambda}{L}$)	Crystallite size, L (nm)
300	4.991106	17.068243	0.0039	0.0013	10.54718
350	4.968098	16.843789	0.0024	0.0014	9.14089
400	4.948012	16.951768	0.0019	0.0016	8.56959
450	4.963096	16.933161	0.0026	0.0017	8.06549

particle size ranges from 100 nm to 5 μm and is appropriate for drug delivery.

3.3 Elemental analysis of CaCO₃ by EDS

The elemental compositions of the samples were characterized using EDS. The energy spectrum of $CaCO_3$ sample was collected from the surface of the sample (red spot in Figure 5a) as shown in Figure 6, which revealed the presence of individual elements in the samples. As shown in Table 3, the samples contained similar elements, namely carbon, calcium, and oxygen, with no significant differences between the elements detected in the four analyzed samples. The EDS analysis also confirms the $CaCO_3$ powders since they exhibit a C/Ca average ratio of approximately 1.05 and an O/C average ratio of approximately 3.243. However, an O/C ratio of 3.630 was observed at the annealing temperature of 400 °C due to the position of collected area.

3.4 Dielectric Property

The dielectric constant measurements were carried out in a frequency range of 10^2 to 10^6 Hz using an RF impedance analyzer: 4191A Dielectric Test Fixture. The ε_r as a function of frequency and annealing temperature of $CaCO_3$ is shown in Figure 7. The values of ε_r are higher in the calcite phase with a clear maximum at the annealing temperature of 300°C. At the frequency of 30 MHz (Figure 8), the values of ε_r are 6.8, 6.1, 6.0 and 6.3 at the annealing temperatures of 300°, 350°, 400°, and 450°C, respectively. These results correspond to the findings reported in the literature[19]. Moreover, the results
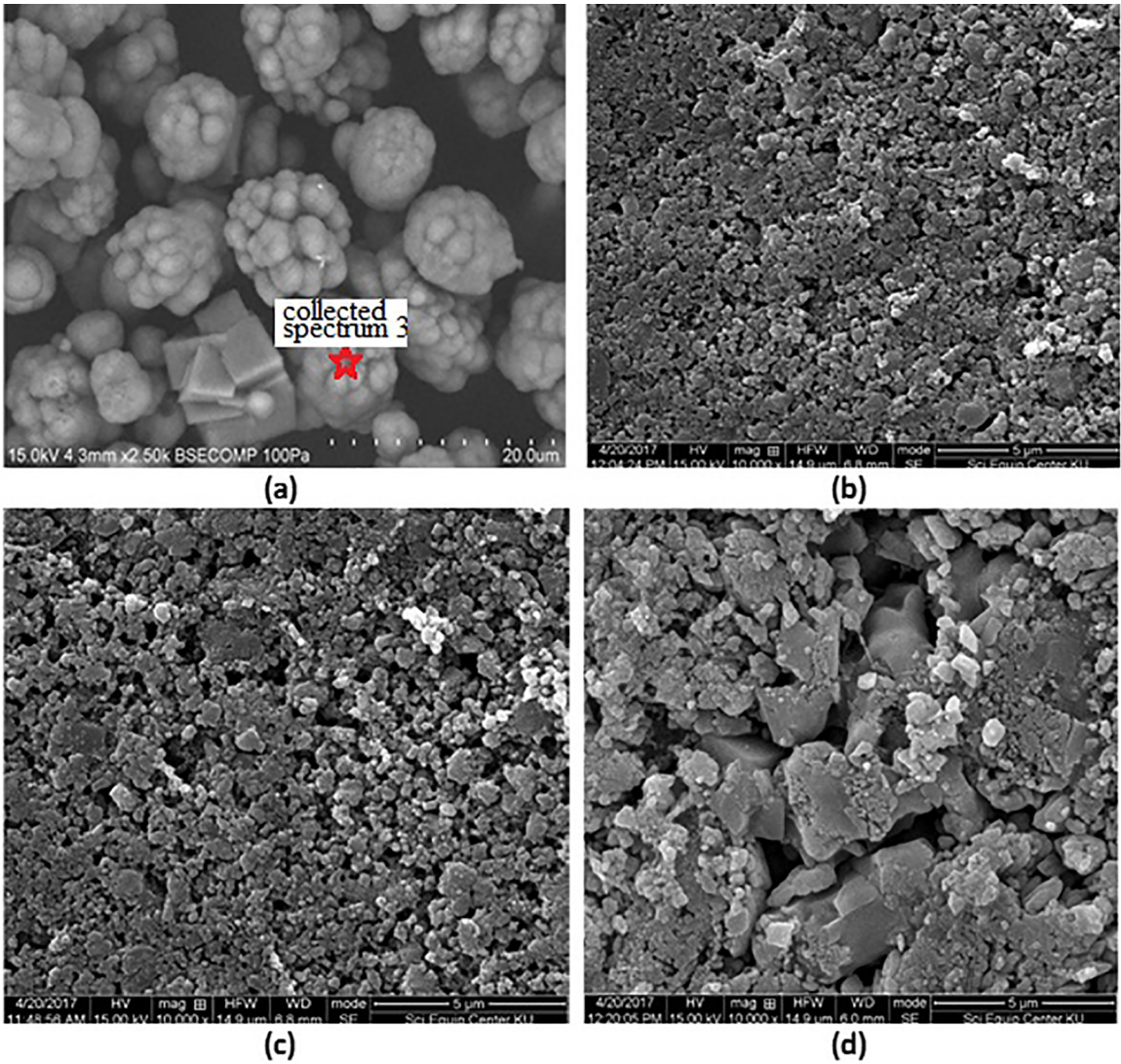
Figure 5. The SEM micrographs of $CaCO_3$ surface, temperature influence on the $CaCO_3$ morphologies; (a) at the reaction temperature of 60°C, (b) at the annealing temperature of 350°C, (c) at the annealing temperature of 400°C, and (d) at the annealing temperature of 450°C
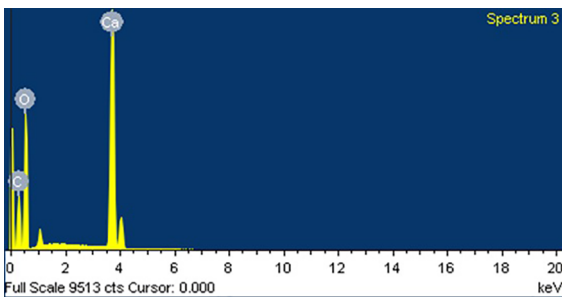

Figure 6. EDX spectral data for $CaCO_3$ at 400°C

show that the dielectric constant decreases as the applied frequency increases. As might be expected from the bulk ceramic data, the trigonal (isometric 32/m) powder shows a much smaller value of ε_r. This is because the polarization contribution is maximized due to many coexisting dipole moments at these voltages. In Figure 7, LC resonances are seen on the dielectric constant as a function of driven

frequency. This is a self-inductance effect on the dielectric measurement[12]. The calculation of self-inductance of a single turn loop depends on loop diameter (D) and diameter size (d) of wire as shown below[20].

$$L_{loop} \approx \mu_0 \mu_r \left(\frac{D}{2} \right) \left(in\left(\frac{8D}{d} \right) - 2 \right) \qquad (12)$$

In this measurement setup, the loop diameter is 300 mm, the wire diameter is 0.5 mm and relative permeability is μ_r $\approx$1. The loop inductance was calculated to be 1.22 μH[20], and this result does not influence the absolute value of the dielectric constant trend line. However, the loop inductance effect could be removed by adjusting the length and the diameter of wires. Dielectric losses of the different annealing temperatures as a function of frequency are shown in Figure

Effect of Temperature Treatment on Electrical Property, Crystal Structures and Lattice Strains of
Precipitated CaCO₃ Nanoparticles

7

Table 3. Elemental composition of desired precipitated $CaCO_3$ at different annealing temperatures

Annealing Temperature	300ºC	
Element	Weight%	Atomic%
C K	12.07	19.84
O K	49.74	61.36
Ca K	38.18	18.80
Ratio of Ca:C:O=1:1.05:3.26	C/Ca=1.055 and O/C=3.09	
Annealing Temperature	**350ºC**	
Element	Weight%	Atomic%
C K	12.64	20.30
O K	51.99	62.68
Ca K	35.38	17.03
Ratio of Ca:C:O=1:1.92:3.68	C/Ca=1.192 and O/C=3.087	
Annealing Temperature	**400ºC**	
Element	Weight%	Atomic%
C K	10.79	17.69
O K	52.04	64.05
Ca K	37.17	18.26
Ratio of Ca:C:O=1:0.968:3.50	C/Ca=0.968 and O/C=3.620	
Annealing Temperature	**450ºC**	
Element	Weight%	Atomic%
C K	12.10	19.66
O K	51.21	62.47
Ca K	36.69	17.87
Ratio of Ca:C:O=1:1.100:3.49	C/Ca=1.100 and O/C=3.177	
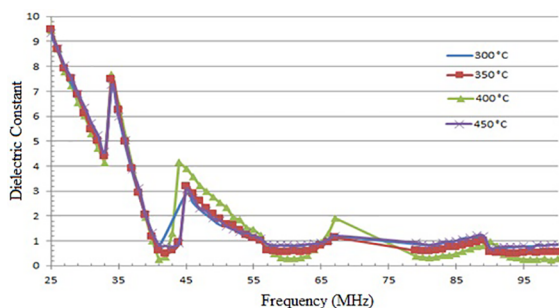
Figure 7. Dielectric properties of $CaCO_3$ with different annealing temperature as a function of driven frequencies.
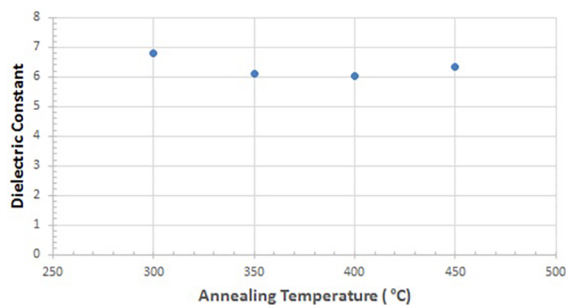
Figure 8. The dielectric constant of $CaCO_3$ with different annealing temperature at 30 MHz.
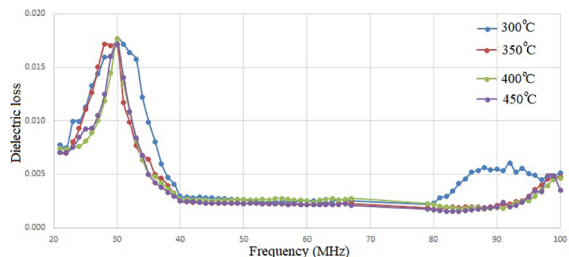
Figure 9. The dielectric loss of $CaCO_3$ with different annealing temperature as a function of driven frequencies.

9. The values of ε'' are the maximum at the frequency of 30 MHz. This result indicates that the $CaCO_3$ samples are dissipated and are in the form of loose materials when it is used in an external electric field.

It can be concluded that the dielectric property of $CaCO_3$ is independent of the annealing temperature. The effect of dielectric properties on drug delivery from $CaCO_3$ corresponds to the drug release profile and delivery mechanism. These properties can be used judiciously to predict drug release and design biomaterials accordingly. This trend is similar to previous reports in the literature[3,9,17].

4. Conclusions

The calcite and vaterite phases of the nanoparticle $CaCO_3$ powders were successfully prepared by the precipitation method. The particle size and morphology of $CaCO_3$ can be controlled by adjusting the reaction temperature in a reflux step of precipitation and annealing temperatures. The vaterite phase can be realized as the reaction temperature increases to 350°C. The crystal formation changes from the cubic-shape and needle-like shape to the round-shape feature at the annealing temperature of 350°C. The crystallite size and the strain deformation of the $CaCO_3$ powders were successfully analyzed by the Scherrer–Gottingen equation. The results show that the crystallite size varies with the annealing temperature while the strain is very small. The $CaCO_3$ powder has a dielectric constant of 6.0–6.8 and quite stable with the increase in annealing temperature. The results of the phase structure, crystallite size, strain deformation, and dielectric constant of the $CaCO_3$ powders are indicative of drug carrier applications.

5. Acknowledgments

6. References

1. Han JT, Xu X, Cho K. Sequential formation of calcium carbonate superstructure: from solid/hollow spheres to sponge-like/solid films. *Journal of Crystal Growth*. 2007;308:110-6.

2. Gao X, Zhu Y, Zhou S, Gao W, Wang Z, Zhou B. Preparation and characterization of well-dispersed waterborne polyurethane/$CaCO_3$ nanocomposites. *Colloids and Surfaces A: Physicochemical and Engineering Aspects*. 2011;377(1-3):312-7.

3. Dinamani M, Kamath PV, Sheshadri R. Electrochemical synthesis of calcium carbonate coatings on stainless substrates. *Materials Research Bulletin*. 2002;37(4):661-9.

4. Somani RS, Patel KS, Mehta AR, Jasra RV. Examination of the polymorphs and particle size of calcium carbonate precipitated using still effluent (i.e., $CaCl_2$ + NaCl Solution) of soda ash manufacturing. *Industrial and Engineering Chemistry Research*. 2006;45(15):5223-30.

5. Declet A, Reyes E, Suárez OM. Calcium carbonate precipitation: a review of the carbonate crystallization process and applications bio inspired composites. *Reviews on Advanced Materials Science*. 2016;44:87-107.

6. Pompe G, Pohlers A, Pötschke P, Pionteck J. Influence of processing conditions on the multiphase structure of segmented polyurethane. *Polymer*. 1998;39(21):5147-53.

7. Khaenamkaew P, Manop D, Tanghengjaroen C, et al. *Effect of reaction temperature on phase transitions and dielectric property of $CaCO_3$ prepared by precipitation method*. In: The 2nd KU SRC Annual National Conference; 2017 aug 30-sep 1; Thailand, Kasetsart University, Si Racha Campus. Thailand, Kartsart: KU SRC; 2017. p. 561-567.

8. Wray JL, Daneils F. Precipitation of calcite and aragonite. *Journal of the American Chemical Society*. 1957;79(9):2031-4.

9. Weitao W, Yu D, Yunchuan X, et al. *Effects of nanoparticle surface treatment on the crystalline morphology and dielectric property of polypropylene/calcium carbonate nanocomposites*. In: Proceeding of the 1st IEEE Internatioal Conference on Nano/Micro Engineering Molecule and System; 2006 aug 18-21; People's Republic of China, Shaanxi Sheng. Republic of China: IEEE; 2006. p. 387-390.

10. Kroon RE. Nanoscience and the Scherrer equation versus the 'Scherrer–Gottingen equation'. *South African Journal of Science*. 2013;109(5-6):1-2.

11. Suryanarayana C, Grant M. *X-ray diffraction: a practical approach*. New York (NY): Springer US; 1998.

12. Griffith DJ. *Introduction to electrodynamics*. 4th ed. Harlow, Essex: New Pearson International; 2014.

13. Keysight Technologies. *Basics of measuring the dielectric properties of materials*. Keysight [Internet]. 2019; [cited 2019 jul 17]. *Available from:* www.keysight.com/find/materials

14. Chen J, Xiang L. Controllable synthesis of calcium carbonate polymorphs at different temperatures. *Powder Technology*. 2009;189(1):64-9.

15. Kim WS, Hirasawa I, Kim WS. Polymorphic change of calcium carbonate during reaction crystallization in a batch reactor. *Industrial and Engineering Chemistry Research*. 2004;43(11):2650-7.

16. Mote VD, Purushotham Y, Dole BN. Williamson-Hall analysis in estimation of lattice strain in nanometer-sized ZnO particles. *Journal of Theorical and Applied Physics*. 2012;6(6):1-8.

17. Sun D, Peng H, Wang S, Zhu D. Synthesis of $CaCO_3$ nanobelts for drug delivery in cancer therapy. *Nanoscale Research Letters*. 2015;10(1):948.

18. Hariharan M, Varghese N, Cherian AB, Sreenivasan PV, Jenish P, Asmy AKA. Synthesis and characterisation of $CaCO_3$ (calcite) nano particles from cockle shells using chitosan as precursor. *American Journal of Scientific and Research Publications*. 2014;4(10):1-5.

19. *Dielectric Constants* of *Common Materials*. *Materials Data sheet – Dielectric Constant Chart*. Kabusa [Internet]. 2007; [cited 2019 jul 17]. *Available from:* https://www.kabusa.com/Dilectric-Constants.pdf

20. *Archambeault B. Understanding inductance in the real-world. Triangle Park, NC, USA:* Interference Technology [Internet]. 2007; [cited 2019 jul 17]. *Available from:* https://interferencetechnology.com/understanding-inductance-real-world/